A&A, 701, A254 (2025)
https://doi.org/10.1051/0004-6361/202556015

Astronomy & Astrophysics

Is ozone a reliable proxy for molecular oxygen?

III. The impact of CH_4 on the O_2–O_3 relationship for Earth-like atmospheres

Thea Kozakis[1,2,⋆], João M. Mendonça[2,3,4], Lars A. Buchhave[2], and Luisa M. Lara[1]

[1] Instituto de Astrofísica de Andalucía – CSIC, Glorieta de la Astronomía s/n, 18008 Granada, Spain
[2] National Space Institute, Technical University of Denmark, Elektrovej, 2800 Kgs. Lyngby, Denmark
[3] School of Physics and Astronomy, University of Southampton, Highfield, Southampton SO17 1BJ, UK
[4] School of Ocean and Earth Science, University of Southampton, Southampton SO14 3ZH, UK

Received 18 June 2025 / Accepted 7 August 2025

ABSTRACT

In the search for life in the Universe, molecular oxygen (O_2) combined with a reducing species, such as methane (CH_4), is considered a promising disequilibrium biosignature. In cases where it would be difficult or impossible to detect O_2 (such as in the mid-IR or low O_2 levels), it has been suggested that ozone (O_3), the photochemical product of O_2, could be used as a proxy for determining the abundance of O_2. As the O_2–O_3 relationship is known to be nonlinear, the goal of this series of papers is to explore how it would change for different host stars and atmospheric compositions and learning how to use O_3 to infer O_2. We used photochemistry and climate modeling to further explore the O_2–O_3 relationship by modeling Earth-like planets with the present atmospheric level (PAL) of O_2 between 0.01% and 150%, along with high and low CH_4 abundances of 1000% and 10% PAL, respectively. Methane is of interest not only because it is a biosignature, but it is also the source of hydrogen atoms for hydrogen oxide (HO_x), which destroys O_3 through catalytic cycles, and acts as a catalyst for the smog mechanism of O_3 formation in the lower atmosphere. We find that varying CH_4 causes changes to the O_2–O_3 relationship in ways that are highly dependent on both the host star and O_2 abundance. A striking result for high CH_4 models in high O_2 atmospheres around hotter hosts is that enough CH_4 is efficiently converted into H_2O to significantly impact stratospheric temperatures, and therefore the formation and destruction rates of O_3. Changes in HO_x have also been shown to influence both the HO_x catalytic cycle and production of smog O_3, causing variations in harmful UV reaching the surface, as well as changes in the 9.6 μm O_3 feature in emission spectra. This study further demonstrates the need to explore the O_2–O_3 relationship in different atmospheric compositions in order to use O_3 as a reliable proxy for O_2 in future observations.

Key words. astrobiology – planets and satellites: atmospheres – planets and satellites: terrestrial planets

1. Introduction

Although ozone (O_3) is not directly created by life, it is still included in discussions about the search for life in the Universe using atmospheric biosignatures. This is because O_3 is the photochemical product of molecular oxygen (O_2), which is primarily produced biologically on modern Earth. However, there are multiple scenarios where O_2 could build up in a planetary atmosphere in the absence of life, so O_2 on its own is not a reliable sign of life (e.g., Hu et al. 2012; Wordsworth & Pierrehumbert 2014; Domagal-Goldman et al. 2014; Tian et al. 2014; Luger & Barnes 2015; Gao et al. 2015; Harman et al. 2015). Instead, O_2 and a reducing species such as methane (CH_4) is thought to be a promising disequilibrium biosignature, as it would require strong surface fluxes of each species, which would be indicative of surface life (e.g., Lovelock 1965; Lederberg 1965; Lippincott et al. 1967).

Ozone enters the conversation because there are scenarios in which O_2 would be difficult or impossible to detect, whereas O_3 would be accessible. For a terrestrial planet with low levels of O_2 (such as on early Earth), it would be difficult to make an O_2 detection, while O_3 is detectable at trace amounts (Kasting et al. 1985; Léger et al. 1993). In addition, while the mid-IR (3–20 μm) holds many opportunities for biosignature searches (Quanz et al. 2022), there are no significant O_2 features, only a collisionally induced absorption feature that is not strong enough for detections of biologically produced O_2 (Fauchez et al. 2020). Therefore, many have suggested using O_3 as a proxy for O_2 in such situations (e.g., Léger et al. 1993; Des Marais et al. 2002; Segura et al. 2003; Léger et al. 2011; Meadows et al. 2018b; Schwieterman et al. 2018).

As O_2 and O_3 are known to have a highly nonlinear relationship (Ratner & Walker 1972; Kasting & Donahue 1980; Kasting et al. 1985; Segura et al. 2003; Gregory et al. 2021; Kozakis et al. 2022; Kozakis et al. 2025), the goal of this series of papers is to explore the O_2–O_3 relationship for a variety of host stars and Earth-like atmospheres in order to gain valuable insight on how to use future observations of O_3 to predict O_2 atmospheric content and potentially identify biosignatures. Here we use the term "Earth-like" to mean a planet with the same planetary parameters as Earth (e.g., radius, gravity), roughly the same atmospheric composition, and an orbital distance from its host star such that it receives the same total amount of flux as on modern Earth. Already we have found that not only is the O_2–O_3 relationship nonlinear, but that it varies significantly depending on the host star and planetary atmospheric composition. In Kozakis et al. (2022) we modeled planets around a variety of host stars with O_2 mixing ratios of 0.01–150% our present atmospheric level (PAL), and in Kozakis et al. (2025) we repeated those same models but with variations of high and low amounts of nitrous

⋆ Corresponding author.

oxide (N_2O). With both studies we found that trends in the O_2–O_3 relationship differ from hotter stars to cooler stars, with the pressure-dependent nature of O_3 formation playing a large role.

In this study, we focus on the impact of CH_4 on the O_2–O_3 relationship and explore how it could impact future observations of O_3. We chose CH_4 not only because it is considered a biosignature (e.g., Thompson et al. 2022), but because it is the source of hydrogen oxides (HO_x) that power catalytic cycles that destroy O_3, as well as processes that create O_3 in the lower atmosphere. Section 2 introduces the relevant atmospheric chemistry, Sect. 3 our methodology, and Sect. 4 our results, including changes in atmospheric chemistry, UV to the ground, and O_3 emission spectra features. In Sect. 5, we discuss the implications of our results, and Sect. 6 provides our main conclusions.

2. Relevant chemistry

2.1. Ozone formation and destruction

The majority of O_3 in the atmosphere of modern Earth is formed in the stratosphere via the Chapman mechanism (Chapman 1930), beginning with O_2 photolysis,

$$O_2 + h\nu \rightarrow O + O \ (175 < \lambda < 242 \text{ nm}), \quad (1)$$

$$O_2 + h\nu \rightarrow O + O(^1D) \ (\lambda < 175 \text{ nm}), \quad (2)$$

which creates either a ground state O atom, or an excited $O(^1D)$ radical depending on the energy of the photon. An $O(^1D)$ radical can either be quenched back to the ground state with the help of a background molecule, M,

$$O(^1D) + M \rightarrow O + M, \quad (3)$$

or react with other species. Oxygen atoms can then combine with O_2 to create O_3,

$$O + O_2 + M \rightarrow O_3 + M. \quad (4)$$

Reaction (4) requires a background molecule to carry away excess energy, meaning that it is a three-body reaction that favors higher pressures. This reaction in particular additionally favors cooler temperatures. Once O_3 has been created, it can be photolyzed to produce O_2 and either ground state O atoms or $O(^1D)$ radicals,

$$O_3 + h\nu \rightarrow O_2 + O(^1D) (\lambda < 310 \text{ nm}), \quad (5)$$

$$O_3 + h\nu \rightarrow O_2 + O \ (310 < \lambda < 1140 \text{ nm}). \quad (6)$$

However, photolysis is not considered a real "loss" of O_3, as the O atom and O_2 molecule created by O_3 photolysis often recombine back into O_3 (Reaction (4)). Because O_3 and O cycle back and forth through photolysis and recombination with O_2, it is useful to keep track of "$O + O_3$", called "odd oxygen." A true loss of O_3 occurs when odd oxygen is converted into O_2,

$$O_3 + O \rightarrow 2O_2, \quad (7)$$

as O_2 photolysis is the limiting reaction of the Chapman mechanism. However, Reaction (7) is not fast, so odd oxygen tends to be destroyed by other methods.

While the Chapman mechanism is the dominant O_3 formation mechanism in the stratosphere, "smog formation" (Haagen-Smit 1952) can create O_3 in the lower atmosphere,

$$OH + CO \rightarrow H + CO_2, \quad (8)$$

$$H + O_2 + M \rightarrow HO_2 + M, \quad (9)$$

$$HO_2 + NO \rightarrow OH + NO_2, \quad (10)$$

$$NO_2 + h\nu \rightarrow NO + O, \quad (11)$$

$$\begin{array}{ll} O + O_2 + M \rightarrow O_3 + M & (4) \\ \hline \text{Net:} \quad CO + 2O_2 + h\nu \rightarrow CO_2 + O_3 & . \end{array}$$

The smog mechanism requires both nitrogen oxides (NO_x, NO_3+NO_2+NO) and hydrogen oxides (HO_x, HO_2+OH+H) as catalysts to form O_3; neither are consumed in the process.

A true loss of odd oxygen/O_3 most typically occurs from catalytic cycles, which take the form,

$$\begin{array}{l} X + O_3 \rightarrow XO + O_2, \\ XO + O \rightarrow X + O_2, \\ \hline \text{Net:} \quad O_3 + O \rightarrow 2O_2 \end{array}$$

with the primary catalytic cycles on Earth being that of the NO_x (X=NO) and HO_x (X=OH) catalytic cycles. The main NO_x catalytic cycle is,

$$NO + O_3 \rightarrow NO_2 + O_2, \quad (12)$$

$$NO_2 + O \rightarrow NO + O_2, \quad (13)$$

with a secondary NO_x catalytic cycle working in the lower stratosphere using NO_3,

$$NO + O_3 \rightarrow NO_2 + O_2, \quad (12)$$

$$NO_2 + O_3 \rightarrow NO_3 + O_2. \quad (14)$$

$$NO_3 + h\nu \rightarrow NO + O_2. \quad (15)$$

The primary mechanism for removing NO_x from the atmosphere is by conversion into stable reservoir species,

$$NO_2 + NO_3 + M \rightarrow N_2O_5 + M, \quad (16)$$

$$OH + NO_2 + M \rightarrow HNO_3 + M, \quad (17)$$

$$HO_2 + NO_2 + M \rightarrow HO_2NO_2 + M. \quad (18)$$

2.2. Methane and HO_x catalytic cycles

Along with the NO_x catalytic cycle the other dominant destruction of O_3 is via the HO_x catalytic cycle. While H_2O is the direct source of HO_x in the atmosphere, H_2O has limited upward transport due to the cold trap, which prevents travel from the troposphere into the stratosphere, hence the significantly drier stratosphere than the troposphere on modern Earth. However, CH_4 can freely move from the ground into the stratosphere, where it can be oxidized into H_2O molecules. As a result, CH_4 is the primary source of stratosphere HO_x, and thus powers the HO_x catalytic cycle.

Another popular biosignature, CH_4, is produced on Earth primarily from natural wetlands, although it has strong anthropogenic sources such as rice paddies and other agricultural processes that are not addressed in this study. When a molecule of CH_4 is transported into the stratosphere, it has the potential to create two H_2O molecules given enough oxygen and incoming UV flux. To start off this process, CH_4 is oxidized by the hydroxyl radical (OH), to create H_2O and the methyl radical CH_3,

$$CH_4 + OH \rightarrow H_2O + CH_3, \tag{19}$$

$$CH_3 + O_2 + M \rightarrow CH_2O + OH + M, \tag{20}$$

$$\begin{aligned} &CH_2O + OH \rightarrow H_2O + CHO, \qquad (21)\\ \text{Net:}\quad &CH_4 + OH + O_2 \rightarrow 2H_2O + HCO \end{aligned}$$

with the net result of two H_2O molecules. Although there is technically a loss of HO_x (through OH), the resulting formyl radical (HCO) is frequently converted back into HO_x via reactions with O_2,

$$HCO + O_2 \rightarrow CO + HO_2. \tag{22}$$

The original source of the OH in Reaction (19) is often via $O(^1D)$ reacting with H_2O,

$$H_2O + O(^1D) \rightarrow OH + OH. \tag{23}$$

Since $O(^1D)$ is created by photolysis with high energy UV photons, production is highly dependent on the spectrum of the host star, which we explore in depth in the rest of this study.

Although on modern day Earth the biggest sink of the short-lived OH radical is CH_4, OH is also the main sink of CH_4 in the atmosphere. Additionally OH is commonly created by $O(^1D)$ resulting from O_3 photolysis, making O_3 an indirect source of HO_x. This creates interesting feedback behavior, as HO_x is a significant sink of O_3 via the HO_x catalytic cycle,

$$OH + O_3 \rightarrow HO_2 + O_2, \tag{24}$$

$$HO_2 + O \rightarrow OH + O_2, \tag{25}$$

in which odd oxygen, $O + O_3$, is converted into two O_2 molecules. In the upper stratosphere, where H atoms are more common (often from H_2O photolysis), odd oxygen can be converted to O_2 via,

$$H + O_2 + M \rightarrow HO_2 + M, \tag{26}$$

$$HO_2 + O \rightarrow OH + O_2, \tag{25}$$

$$OH + O \rightarrow H + O. \tag{27}$$

In the lower stratosphere where there is less O_2 photolysis and therefore fewer O atoms, odd oxygen is destroyed via,

$$OH + O_3 \rightarrow HO_2 + O_2, \tag{28}$$

$$HO_2 + O_3 \rightarrow OH + 2O_2. \tag{29}$$

There are multiple reactions that destroy either OH or HO_2, but they are typically recycled back into another HO_x species. Photolysis is also not a true sink of HO_x since HO_2 photolysis creates OH, and OH is too short-lived for significant photolysis. Efficient methods of HO_x destruction are conversion to H_2O,

$$OH + HO_2 \rightarrow H_2O + O_2, \tag{30}$$

since the conversion of H_2O into HO_x is a limiting reaction. HO_x is also lost via conversion to a stable reservoir species,

$$OH + OH + M \rightarrow H_2O_2 + M, \tag{31}$$

$$OH + NO_2 + M \rightarrow HNO_3 + M, \tag{17}$$

$$HO_2 + NO_2 + M \rightarrow HO_2NO_2 + M. \tag{18}$$

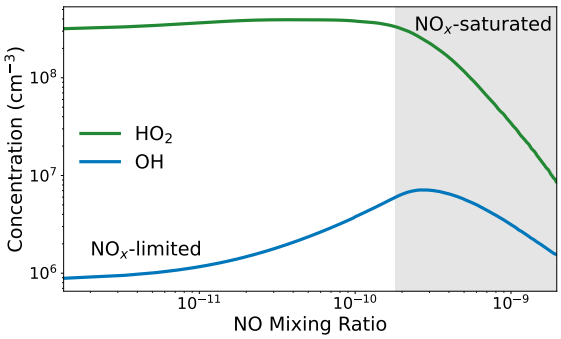

Fig. 1. Relationship between NO_x and HO_x in the lower atmosphere on modern Earth, adapted from Logan et al. (1981). In the NO_x-limited regime (white background) an increase of NO_x will lead to an increase of HO_x and thus increased productivity of the smog mechanism. In the NO_x-saturated regime (gray background) the NO_x/HO_x ratio reaches a tipping point where NO_x begins to deplete HO_x by locking it up into stable reservoir species, therefore suppressing smog formation.

2.3. Relationship between NO_x and HO_x

As mentioned previously, O_3 is often an indirect source of HO_x as $O(^1D)$ radicals that react with H_2O to form HO_x (Reaction (23)) are typically formed via O_3 photolysis (Reaction (5)) in O_2-rich atmospheres. This causes an interesting relationship with the smog mechanism of O_3 production (Reactions (4), (8), (9), (10), (11)), as both HO_x and NO_x are required as catalysts. Earth-based studies have found that the amount of NO_x present in a region can either increase the rate of smog produced O_3 (and thus indirectly increasing HO_x) or suppress O_3 production by locking HO_x up into reservoir species such as HNO_3 (Reaction (17)) or HO_2NO_2 (Reaction (18)). We refer to these two scenarios in which NO_x can assist smog production or hinder it as the "NO_x-limited" and "NO_x-saturated" regimes, respectively, as illustrated in Fig. 1. In the NO_x-limited regime, increasing NO_x leads to more O_3 and therefore more HO_x, encouraging smog formation, and in the NO_x-saturated regime, the NO_x/HO_x ratio has become high enough that NO_x locks up HO_x in reservoir species and suppresses smog formation.

However, it is important to note that these regimes have been studied primarily in the context of NO_x pollution on modern Earth via anthropogenic activities, where the emphasis is placed on how changes in NO_x (not changes in HO_x) impact smog O_3 formation. This study provides a new perspective on these NO_x regimes, as we focus on changes in HO_x caused by varying CH_4 levels. These regimes were discussed in depth in Kozakis et al. (2025) where we varied N_2O (and therefore NO_x) and we found that even for modern levels of N_2O and O_2 the NO_x abundances

were already high enough to be in the NO_x-saturated regime for planets around all hosts explored in this paper except for the M5V at modern O_2 levels, causing severe suppression of the smog mechanism.

3. Methods

3.1. Atmospheric models

We used `Atmos`[1], a publicly available 1D coupled photochemistry and climate code to model the atmospheres of Earth-like planets, following Kozakis et al. (2022) and Kozakis et al. (2025). We briefly describe the code and our chosen parameters here, and refer the reader to other sources for a full description (Arney et al. 2016; Meadows et al. 2018a; Kozakis et al. 2022). Inputs to `Atmos` require a stellar host spectrum (121.6–45 450 nm), planetary parameters (e.g., radius, gravity), and the initial composition of the atmosphere and boundary conditions.

For the photochemistry code (Kasting 1979; Zahnle et al. 2006) we used the modern Earth template available with `Atmos`, including 50 gaseous species and 233 chemical reactions. The atmosphere is broken up into 200 plane parallel layers from the planetary surface to 100 km, with the flux and continuity equations solved simultaneously in each individual layer. Vertical transport is included for long-lived species, as well as molecular and eddy diffusion. Radiative transfer is calculated using a δ-2-stream method (Toon et al. 1989), and the code is considered to be converged when the length of the adaptive time step reaches the age of the universe within the first 100 steps.

The climate code (Kasting & Ackerman 1986; Kopparapu et al. 2013; Arney et al. 2016) then uses the atmospheric composition calculated in the photochemistry code along with the incoming stellar flux to calculate temperature and pressure profiles for the atmosphere. Here the atmosphere is broken up into 100 layers from the surface up until 1 mbar (typically <60–70 km), as the code does not run reliably at lower pressures (Arney et al. 2016). When transferring information back to the photochemistry code pressures above 1 mbar hold the temperature constant. Each layer uses a δ-2-stream multiple scattering method to calculate stellar flux absorption. A correlated-k method is used for outgoing IR for O_3, H_2O, CH_4, CO_2, and C_2H_6 with single and multiple scattering. Convergence is reached when the temperature and flux differences out of the top of the atmosphere are considered small enough ($\sim<10^{-5}$) (Arney et al. 2016).

For this study we iterated the photochemistry and climate codes back and forth 30 times and utilized the short-stepping technique for better climate code convergence (Teal et al. 2022; Kozakis et al. 2022). Our planets had the same radius and gravity as Earth, and orbited their host stars at the Earth-equivalent distance where they received the same total amount of flux as modern Earth. Fixed mixing ratio abundances of O_2 were varied from 0.01% to 150% PAL while additionally varying CH_4 (see Table 1). We considered fixed CH_4 mixing ratios of 10% and 1000% PAL for high and low CH_4 scenarios (same as N_2O in Kozakis et al. 2025) to continue exploring the parameter space of possible Earth-like atmospheres and the resulting impact on the O_2–O_3 relationship. We note that for our high CH_4 models that the CH_4/CO_2 ratio is not high enough for haze formation (Arney et al. 2016), and it is therefore not considered in this study. Other relevant gaseous species held at constant mixing ratios of their present atmospheric levels are N_2O (3.0×10^{-6}), H_2 (5.3×10^{-7}), and CO (1.1×10^{-7}).

Table 1. Model parameters.

Model name	CH_4 MR	O_2 MR
Kozakis et al. (2022)	1.8×10^{-6}	2.1×10^{-5}–0.315
Low CH_4 (10% PAL)	1.8×10^{-7}	2.1×10^{-5}–0.315
High CH_4 (1000% PAL)	1.8×10^{-5}	2.1×10^{-5}–0.315

Notes. Abbreviations: MR = mixing ratio; PAL = present atmospheric level.

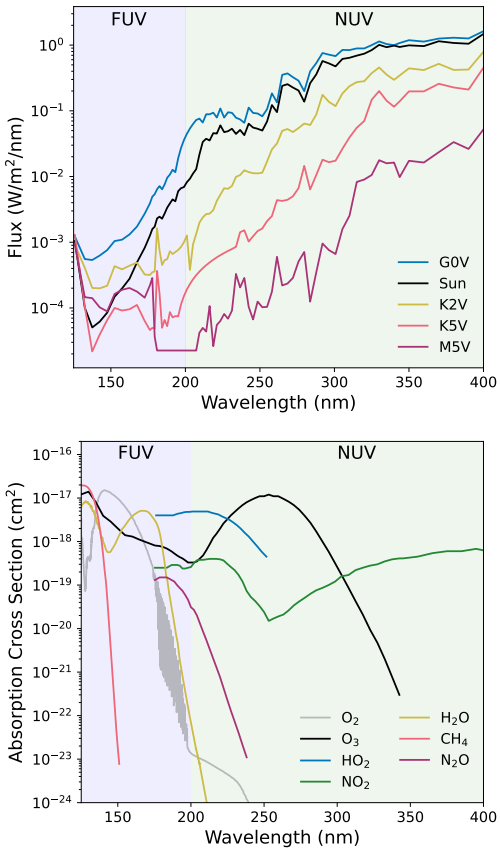

Fig. 2. Stellar spectra for the host stars following Kozakis et al. (2022) (top) along with the cross-sections used by `Atmos` of relevant species (bottom). The ratio of far-UV (FUV) to near-UV (NUV) flux is important in driving atmospheric chemistry, and is indicated by the colored backgrounds. The abrupt cutoff of NO_2, N_2O, and HO_2 cross-sections is due to the extremely low photolysis rates of those species at shorter wavelengths due to absorption from other atmospheric species (i.e., CO_2).

3.2. Input stellar spectra

For host stars we used the same stellar spectra as in Kozakis et al. (2022) and Kozakis et al. (2025), shown in Fig. 2 along with absorption cross-sections of relevant species. For the G0V-K5V hosts the UV data came from *International Ultraviolet Explorer* (IUE) data archives[2] combined with synthetic ATLAS data for visible and IR wavelengths (Kurucz 1979). Our M5V host is

[1] https://github.com/VirtualPlanetaryLaboratory/atmos

[2] http://archive.stsci.edu/iue

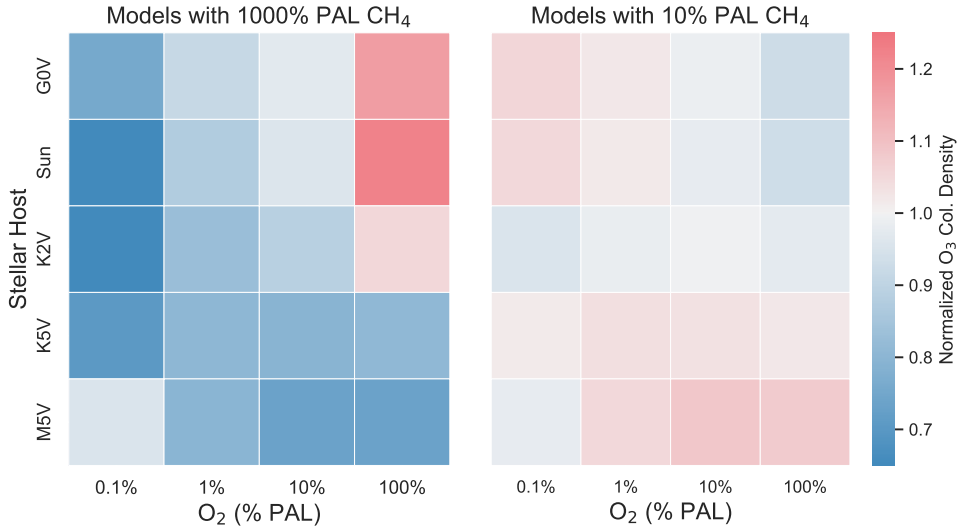

Fig. 3. Ozone abundances normalized to the amount produced at modern levels of CH_4 for both the high (left) and low (right) CH_4 models for all host stars at 0.1%, 1%, 10%, and 100% PAL O_2. The most striking result is that for the high CH_4 models there is less O_3 compared to modern CH_4, except for planets around the hottest hosts at 100% PAL O_2. This is due both to the indirect impact of CH_4 on the stratospheric temperature, as well as a boost in the smog mechanism due to a decreased NO_x/HO_x ratio. The rest of the cases for the CH_4 models show increased O_3 depletion due to a higher amount of CH_4 from the increased efficiency of the HO_x catalytic cycle's ability to destroy O_3.

GJ 876 from the Measurements of the Ultraviolet Spectral Characteristics of Low-mass Exoplanetary Systems (MUSCLES) survey (France et al. 2016). For full details of all host star spectra, see Rugheimer et al. (2013) and Kozakis et al. (2022).

3.3. Post-processing radiative transfer models

To explore the observational impacts of the changing O_2–O_3 relationship, we used the Planetary Intensity Code for Atmospheric Scattering Observations (`PICASO`) to simulate planetary emission spectra, using model atmosphere results from `Atmos` following Kozakis et al. (2022). `PICASO`[3] (Batalha et al. 2019, 2021) is a publicly available code capable of simulating transmission, reflectance, and emission spectra, using atmospheric composition and temperature/pressure profiles calculated by atmospheric modeling codes. We simulated our model planets at full phase (0°) from 0.3 to 14 μm, and focused in particular on the 9.6 μm O_3 feature. We note that although it is unlikely for a planet to be imaged at full phase, it should not have a significant impact on mid-IR for a planet with minimal day-to-day temperature contrast.

4. Results

We found that the impact of CH_4 on the O_2–O_3 relationship cannot be generalized, as it changes depending on the host star and the amount of O_2. In Sect. 4.1 we explored the impact on atmospheric chemistry, changes in UV to the ground in Sect. 4.2, and impact on simulated planetary emission spectra in Sect. 4.3. Supplementary figures and tables are available in Appendix A.

4.1. Atmospheric chemistry

4.1.1. Atmospheric chemistry: Overview

Overall planet models were affected more by the high CH_4 models than the low CH_4 models, with higher CH_4 either depleting or increasing the total O_3 abundance compared to atmospheres with modern levels of CH_4 depending on the host star and O_2 level, as seen in Figs. 3 and 4. The greatest increase in O_3 from different CH_4 levels was experienced by the Sun-hosted planet with the high CH_4 model at 100% O_2 PAL, resulting in 122% of the original O_3 abundance. The most O_3 depletion also occurred with the high CH_4 models but for the K2V-hosted planet at 0.1% PAL O_2 where it retains only 62% of the original O_3 abundance.

An initially striking result is that for the high CH_4 models planets around all host stars at all O_2 levels display O_3 depletion when compared to models with modern levels of CH_4, except for those around the hottest host stars (G0V-K2V) at O_2 levels similar to modern Earth. The increased O_3 for the high CH_4 models around hotter hosts (as well as the decreased O_3 for the corresponding cases with the low CH_4 models) might seem counterintuitive as CH_4 is the parent molecule for HO_x, which catalytically destroys O_3 (Sect. 2.2). Indeed, HO_x species are consistently more abundant with all high CH_4 models, powering more efficient HO_x catalytic cycles that destroy O_3. The main processes affecting the O_2–O_3 relationship when varying CH_4 abundance are:

- the amount of stratospheric H_2O and HO_x created by CH_4,
- indirect effects of CH_4 on stratospheric temperature,
- smog mechanism efficiency as NO_x/HO_x ratio changes,
- changing HO_x/O_3 ratio at different O_2 levels.

We go into detail on each of these processes in the following subsections.

4.1.2. Atmospheric chemistry: Efficiency of converting CH_4 to HO_x

As summarized in Sect. 2.2, a CH_4 molecule can be converted into two H_2O molecules (Reactions (19), (20), (21)) given enough UV light and oxygen to power this process. In particular, OH, which begins this reaction chain, is formed by the $O(^1D)$ radical reacting with H_2O (Reaction (23)), which is created via photolysis,

$$O_2 + h\nu \rightarrow O + O(^1D)\ (\lambda < 175\ \text{nm}), \quad (2)$$

[3] https://natashabatalha.github.io/picaso/index.html

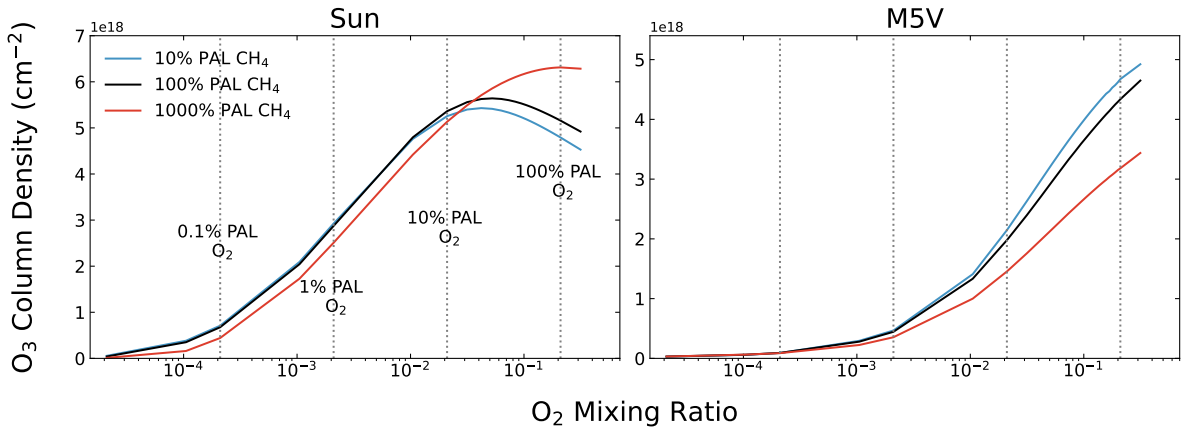

Fig. 4. Absolute values of the O_2–O_3 relationship at all O_2 and CH_4 levels modeled for planets around the Sun (left) and M5V (right) hosts. O_2 levels of 0.1%, 1%, 10%, and 100% PAL are marked with vertical dashed lines to enable easier comparison with Fig. 3. This figure highlights the stark difference in how CH_4 impacts the O_2–O_3 relationship differently for hotter and cooler host stars, due primarily to the amount of UV flux arriving at the planet. For hotter hosts the higher UV flux allows more efficient conversion of CH_4 into H_2O and then HO_x compared to the lower UV flux of M5V host. Full O_2–O_3 relationships of all hosts including comparisons to Kozakis et al. (2025) are located in Appendix A.

$$O_3 + h\nu \rightarrow O_2 + O(^1D)\ (\lambda < 310\ \text{nm}), \quad (5)$$

$$N_2O + h\nu \rightarrow N_2 + O(^1D)\ (\lambda < 200\ \text{nm}), \quad (32)$$

$$CO_2 + h\nu \rightarrow CO + O(^1D)\ (\lambda < 167\ \text{nm}), \quad (33)$$

allowing planets with high amounts of incoming UV flux to be more efficient at converting CH_4 into H_2O. In addition, the main source of $O(^1D)$ radicals is typically from O_3 photolysis (as it can be photolyzed at longer wavelengths than the other options), which causes the conversion of CH_4 into H_2O to favor oxygen-rich environments. Due to the UV and oxygen requirements, conversion rates of CH_4 into H_2O and then into HO_x are faster for planets around hosts with higher UV flux at higher O_2 levels.

The higher levels of HO_x that the high CH_4 models bring cause faster HO_x catalytic cycles that destroy O_3. However, planets around the 3 hottest hosts at 100% PAL O_2 experience an increase in O_3 for the high CH_4 models, despite the fact that they are the hosts converting the most CH_4 into HO_x. The reason behind this O_3 increase is due to the indirect impact of CH_4 on stratospheric temperature, and the efficiency of the smog mechanism for planets around those hosts with high amounts of HO_x.

4.1.3. Atmospheric chemistry: Indirect impact of CH_4 on stratospheric temperature

Planets around hotter hosts at high O_2 levels are the most efficient at converting CH_4 into HO_x, but also into H_2O. Although this increases the amount of H_2O converted into HO_x, another effect of the large amount of stratospheric H_2O is that it forms at a high enough altitude to have a cooling effect. Unlike in the troposphere, where H_2O heats the atmosphere as a greenhouse gas, in the stratosphere H_2O radiates heat into space, similar to CO_2 stratospheric cooling seen on modern Earth (Goessling & Bathiany 2016; Santer et al. 2023). In the stratosphere, H_2O radiates more in the infrared than absorbs energy coming from the lower atmosphere, resulting in a net cooling. This causes atmospheres with enough excess H_2O to experience significant stratospheric cooling, especially for planets with hotter hosts at high O_2 as shown in Fig. 5. For the low CH_4 cases the opposite occurs where there is less stratospheric H_2O, causing a warmer stratosphere when compared to modern levels of CH_4, although the effect is smaller than for the high CH_4 cases.

Stratospheric cooling caused by excess H_2O for the hottest hosts at high O_2 causes two main changes in the O_3 abundance:
- a faster Chapman mechanism and faster O_3 production,
- a slower NO_x catalytic cycle and slower O_3 destruction.

Stratospheric cooling from increased H_2O abundance occurs for a range of O_2 levels for the planets around the G0V and Sun hosts, but only to the extent that it overcomes the depletion of O_3 from the faster HO_x catalytic cycles at high O_3 with high CH_4.

4.1.4. Atmospheric chemistry: Smog mechanism efficiency with changing HO_x

In addition to the faster O_3 production and slower O_3 destruction due to stratospheric cooling from excess H_2O with the high CH_4 models, planets hosted by the hottest stars also experience a boost in O_3 production from the smog mechanism. Although HO_x is not directly created or consumed by the smog mechanism (Reactions (4), (8), (9), (10), (11)), it is necessary to the process as a catalyst. As discussed in both Sects. 2.1 and 2.3, at high enough levels of NO_x the atmosphere will enter the NO_x-saturated regime and NO_x will begin to deplete HO_x by converting it into reservoir species (see Fig. 1). Planets around hotter stars (G0V-K2V) in particular have enough NO_x in their lower stratospheres to place them in the NO_x-saturated regime for modern levels of N_2O, resulting in significant HO_x depletion.

In Kozakis et al. (2025) we determined which NO_x regime an atmosphere was in by looking at the NO_x abundance, but in this study we took a different approach because it is HO_x, not NO_x, that has significant variation. In environments where there are greatly increased levels of HO_x, we find that the cut-off of NO_x that determines the NO_x-saturated and NO_x-limited regimes changes. It is seen in Fig. 6 for the planet around the Sun at 100% PAL O_2 with the high CH_4 models that there is a significant decrease in depletion of HO_2 caused by high NO_x when compared to models with modern levels of CH_4. Although the planet around the Sun at modern levels of O_2 and NO_x was squarely in the NO_x-saturated regime, since the NO_x/HO_x ratio is smaller with the increased CH_4 there is significantly less HO_2 depletion indicating that the atmosphere has been pushed toward the NO_x-limited regime. We see evidence of this occurring for

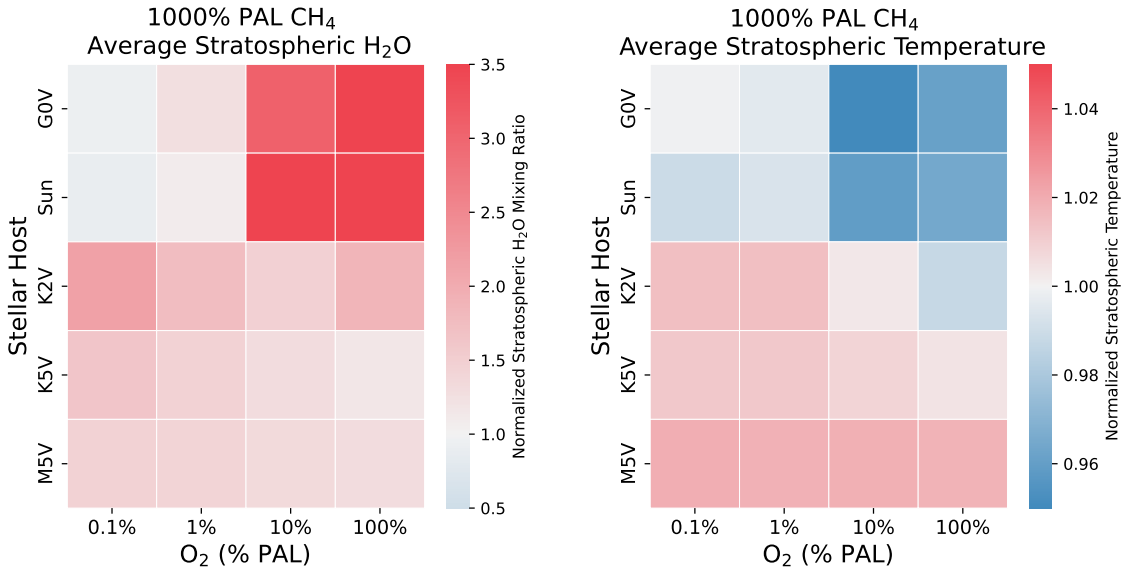

Fig. 5. Average stratospheric H_2O (left) and temperatures (right) for high CH_4 models all normalized to results from models using modern levels of CH_4. Nearly all models experience an increase in H_2O for the high CH_4 models due to the conversion of CH_4 into H_2O in the stratosphere. Planets around hotter hosts with higher O_2 show the largest increases as incident UV and O_2 are necessary for creating H_2O in this scenario. The excess H_2O impacts the temperature, providing stratospheric cooling in cases with large increases of H_2O. As the atmosphere is thin in the stratosphere heat radiating from H_2O can escape to space, causing an effect similar to stratospheric CO_2 cooling present on modern Earth.

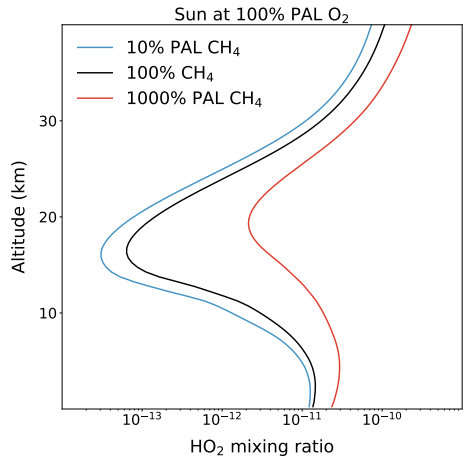

Fig. 6. Profiles of HO_2 for the planet around the Sun at 100% PAL O_2 and different levels of CH_4. The significant HO_2 depletion present for low and modern levels of CH_4 is lessened for the high CH_4 models. This is because the HO_2 depletion is due to the Sun-hosted planet being in the NO_x-saturated regime, but increased CH_4 allows enough HO_x production to lessen this effect.

the G0V, Sun, and K2V hosts at O_2 levels near 100% PAL O_2 with the high CH_4 models, resulting in a boost of smog mechanism-produced O_3. This is the other part of the puzzle as to why planets around these hosts experience an increase in O_3 with the high CH_4 models at modern O_2 levels.

The smog mechanism is also the reason that the M5V-hosted planet with the high CH_4 models experiences less O_3 depletion as O_2 levels decrease, as opposed to planets around all other hosts which experience more O_3 depletion with decreasing O_2. The planet around the M5V host is the only one to always exist in the NO_x-limited regime, and therefore does not suffer from suppression of the smog mechanism as do planets around the other hosts. In addition, smog formation becomes even more efficient at lower O_2 levels as HO_x is "pushed" closer to the ground as UV shielding from O_2 and O_3 decreases. Photolysis allows HO_x to form deeper in the atmosphere, allowing the lower atmosphere HO_x to speed up smog formation even further (see Kozakis et al. 2022 for a longer discussion of this process). This effect occurs for planets around all host stars, but unlike planets around other hosts, for the M5V-hosted planet the extra O_3 produced from the smog mechanism has a more significant impact on the O_2–O_3 relationship since smog-produced O_3 makes up a much larger portion of the total O_3 abundance. This is because the Chapman mechanism has a photon requirement of less than 242 nm for O_2 photolysis, whereas the smog mechanism can be fulfilled with near-UV and visible photons for the required NO_2 photolysis (see Figure 2). The low UV flux of the M5V host allows the smog mechanism to take on a larger role in O_3 production than for planets around hotter hosts. For this reason for the high CH_4 models with the M5V-hosted planet the amount of O_3 depletion decreases with decreasing O_2. As the amount of Chapman-produced O_3 from O_2 photolysis decreases, increased amounts of smog-produced O_3 from added HO_x are more significant.

4.1.5. Atmospheric chemistry: Changing HO_x/O_3 ratio

For planets around all hosts other than the M5V as the O_2 level decreases, a larger portion of O_3 is depleted. This is because as O_2 abundance decreases, the HO_x/O_3 ratio increases. As discussed in Sect. 4.1.2, conversion from CH_4 into HO_x is more efficient at higher O_2 levels as O_3 is often an indirect source of HO_x. Formation of HO_x occurs when H_2O reacts with $O(^1D)$ radicals, which are most easily formed from O_3 photolysis when there is sufficient O_3 supply, as O_3 can be photolyzed by much longer wavelength photons than the other suppliers of $O(^1D)$: O_2, N_2O, and CO_2 (Reactions (2), (5), (32), (33)). However, when O_3 (and O_2) levels decrease, HO_x begins to source $O(^1D)$ radicals more from photolysis of N_2O and CO_2. Although this requires higher energy photons, it is also easier for these species

to be photolyzed deeper into the atmosphere as O_2 and O_3 levels decrease (causing less UV shielding), thus creating a larger HO_x/O_3 ratio with decreasing O_2. With a higher HO_x/O_3 ratio the HO_x catalytic cycle has an easier time depleting O_3 at these lower O_2 levels. As discussed in the previous section (Sect. 4.1.4) this effect of increasing amounts of O_3 depletion occurring at lower O_2 levels does not occur for the M5V-hosted planet due to the boost in smog-produced O_3.

4.2. UV to ground

Variations in O_3 caused by different CH_4 abundances resulted in varying amounts of UV shielding in the atmosphere, and therefore different amounts of UV flux reaching the surface of our model planets. The level of potential biological damage that UV photons can inflict is dependent on wavelength, described by three UV regimes that we used here. UVA (315–400 nm) is the lowest energy UV and least dangerous, and is not shielded by O_3; UVB (280–315 nm) is responsible for skin tanning and skin cancer, and is partially shielded by O_3; and lastly UVC (121.6–280 nm) is capable of significant biological harm, but is fortunately well shielded by O_3 and O_2, assuming that they exist in significant quantities in the atmosphere. Along with being the most dangerous, UVC surface flux also has a highly nonlinear relationship with the amount of O_3 in the atmosphere, as it is UVC flux (<242 nm; Reactions (1), (2)) that is necessary for the Chapman mechanism to produce O_3. Results for UVC surface flux variations at 100%, 10%, 1%, and 0.1% PAL O_2 are shown in Fig. 7, along with a table for UVB and UVC results in the Appendix (Table A.1). As in Kozakis et al. (2022) UVA surface flux did not vary with changing O_2 or CH_4 values (always ~80% reaching the surface) so it is not discussed here.

As UVB flux is partially shielded by O_3, varying CH_4 causes changes to the amount of UVB photons reaching the ground in some cases, but only very slightly. The largest decrease was for the Sun-hosted planet at 100% PAL O_2 with the high CH_4 models having only 80% of the original UVB surface flux due to increased O_3 shielding. The largest increase in UVB surface flux was also at 100% PAL O_2 for the high CH_4 models, but this time with the M5V-hosted planet receiving 124% the UVB surface flux that it did with modern levels of CH_4. For O_2 levels under 100% PAL changes in the amount of UVB flux arriving at the surface changed only slightly, with larger effects being seen consistently with the high CH_4 models due to the larger impact on O_3 formation and destruction (see Table A.1).

Changes in UVC surface flux were much more significant, due to the larger absorption cross-sections at these wavelengths. The highest increases and decreases of UVC surface flux corresponded to the same models with the largest UVB surface flux differences: the planets around the Sun and M5V hosts, both for the high CH_4 models at 100% PAL O_2. The planet around the Sun experienced a factor of just 7.5×10^{-5} times the original UVC flux at modern levels of CH_4 due to the increased amounts of O_3 caused by stratospheric cooling, decreased NO_x catalytic cycle efficiency, and extra smog production. The largest increase in UVC surface flux from the planet around the M5V host (receiving a factor of 2.1×10^4 more) was due to the increased ability for the HO_x catalytic cycle to destroy O_3. For the low CH_4 models the largest variations in UVC surface flux were similarly at 100% PAL O_2 with the largest increase in surface UVC for the planet around the Sun with a factor of 22 times more UVC surface flux, and the largest decrease was for the M5V-hosted planet having 5.8×10^{-2} times the original UVC flux due to the decreased ability of the HO_x catalytic cycle to destroy O_3. For lower oxygen levels the variation in O_3 was significantly decreased, causing the variation in UVC surface flux to be minimized, with the amount of UVC flux variation compared to modern CH_4 levels not exceeding an order of magnitude.

4.3. Planetary emission spectra

We additionally generated planetary emission spectra to explore the potential impact on future observations that varying CH_4 could have on the 9.6 μm O_3 feature. Emission spectral features are highly influenced by the temperature difference between the emitting and absorbing layers of the atmosphere, which as shown in Kozakis et al. (2022) is particularly relevant when considering O_3 features. Since O_3 NUV absorption is the primary source of stratospheric heating on modern Earth, there is a counterintuitive effect where a planet with large amounts of O_3 can have a shallower emission feature than a planet with significantly less O_3. This is because a planet experiencing stratospheric heating via O_3 will have a decreased temperature difference between the planetary surface and stratosphere, resulting in a shallower emission spectral feature depth. However, this will only happen for planets receiving sufficient NUV flux from their host, as this is required for said stratospheric heating to occur. This is shown in the left panel of Fig. 8, where variations in the 9.6 μm O_3 feature from just varying O_2 in Kozakis et al. (2022) are shown. For a more detailed discussion of this phenomena, see Kozakis et al. (2022).

Once again it the high CH_4 models had more of an impact than the low CH_4 models (see Fig. 8). Planets around hotter hosts experienced the most variability in the O_3 feature due to different CH_4 and O_2 abundances, owing to the indirect impact of CH_4 on stratospheric temperature. For planets that experienced stratospheric cooling from high H_2O content, O_3 spectral features are much deeper both because of increased O_3 abundance, but also from the larger temperature difference between the emitting and absorbing layers of the atmosphere. However, at lower O_2 levels for planets around these same hosts the O_3 features became shallower than with modern CH_4 abundances, due to lower O_3 abundances from the higher destruction rates of O_3 via more productive HO_x catalytic cycles. For all other cases the high CH_4 models resulted in shallower O_3 spectral features, again due to the decreased amounts of O_3 from the higher efficiency of the HO_x catalytic cycle. Stratospheric temperatures did not vary significantly in these cases, leading to changes in the O_3 feature depth corresponding more directly to changes in O_3 abundance. It is also worth noting that atmospheres with the high CH_4 models had generally hotter surface temperatures and atmospheres as CH_4 is a greenhouse gas. Overall feature depth changed the most for planets around the G0V and Sun hosts with the high CH_4 models, as they experienced significant deepening of features at high O_2 levels, and much shallower features at low O_2 levels.

5. Discussion

5.1. Comparison to impact of N_2O on the O_2–O_3 relationship

This paper is in many ways a "sister study" to Kozakis et al. (2025), which varied N_2O instead of CH_4 in order to understand how it would impact the O_2–O_3 relationship. Both N_2O and CH_4 are potential biosignatures (Schwieterman et al. 2018; Schwieterman et al. 2022; Thompson et al. 2022; Angerhausen et al. 2024), power the primary catalytic cycles (with NO_x and HO_x), and influence the smog mechanism of O_3 formation. However, we found that Earth-like atmospheres experience different

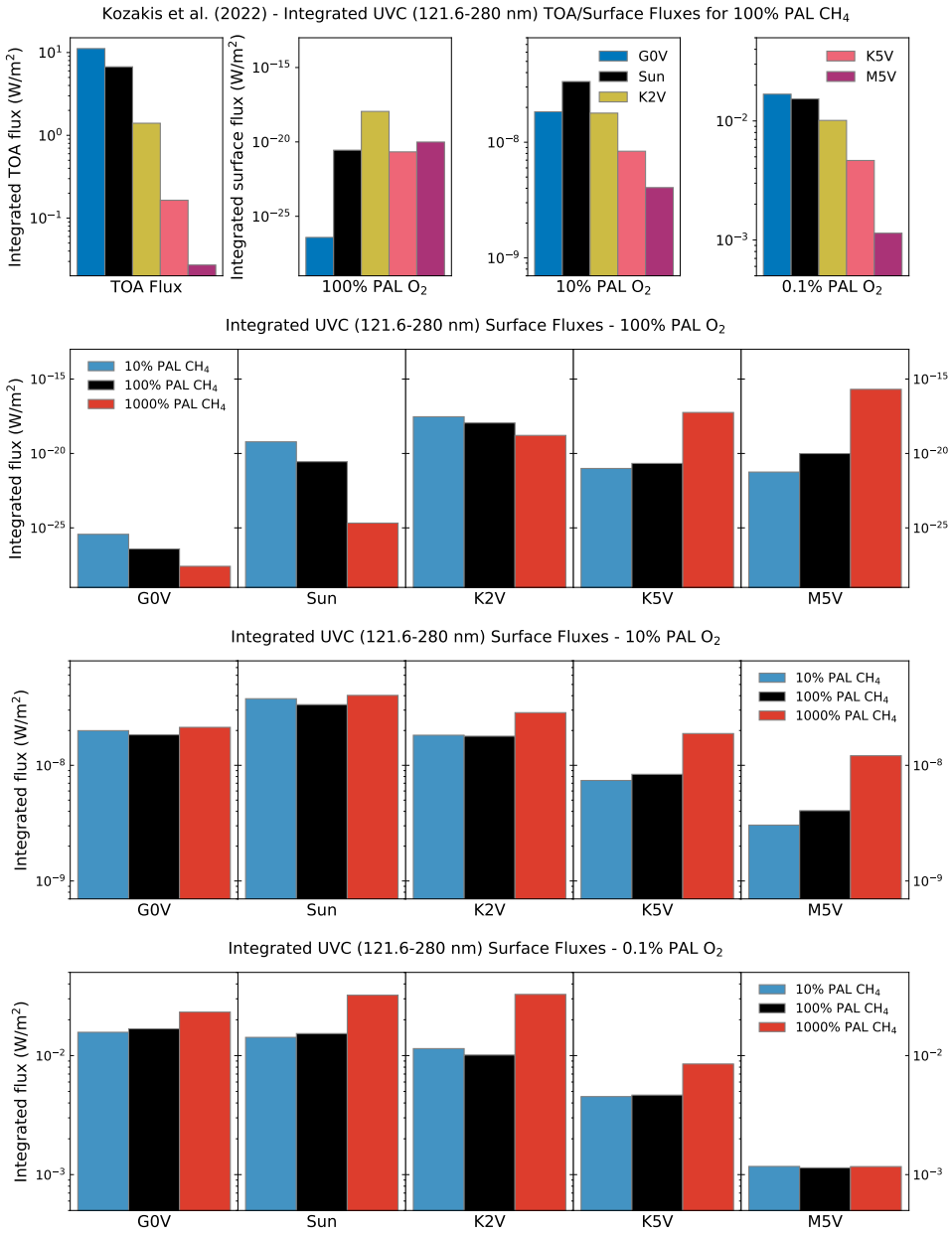

Fig. 7. Comparisons of UVC results with modern CH_4 abundances (top row) with incident top-of-atmosphere (TOA) UVC flux and surface UVC flux for all hosts with modern levels of CH_4 at different O_2 levels, and surface UVC flux with varying CH_4 for 100% PAL O_2 (second row), 10% PAL O_2 (third row) and 0.1% PAL O_2 (bottom row). Surface UVC plots from Kozakis et al. (2022) use the same y-axis limits as the corresponding plots in the bottom three rows to enable easier comparison. Changes in UVC surface flux are most significant for 100% PAL O_2 due to the dependency of oxygen to convert CH_4 into H_2O and HO_2.

responses to variations and N_2O and CH_4, depending on both the amount of O_2. As the ultimate goal of this paper series is to explore and navigate the challenges of using O_3 as a proxy for O_2, it is useful to compare how N_2O and CH_4 impact the O_2–O_3 relationship differently. Figures comparing results from Kozakis et al. (2025) and this study are located in Appendix A.

Overall at higher O_2 levels (> ~1% PAL O_2) varying N_2O had a stronger impact on the total amount of O_3 for planets around all stars except for the M5V host, due to changing efficiency of the NO_x catalytic cycle (Fig. A.1). For the high N_2O models at high O_2 the depletion of O_3 was the most extreme, causing orders of magnitude differences in harmful UVC flux reaching the ground – significantly larger changes than when varying CH_4 (Fig. A.3 and Table A.1). For lower O_2 levels high CH_4 led to O_3 depletion, while high N_2O resulted in increased O_3 formation from a boost to the smog mechanism. Changes in the O_3 abundance at these lower O_2 levels from the low N_2O and CH_4 models were much smaller. Both N_2O and CH_4 were found to impact the smog mechanism, demonstrating in different scenarios the importance of the NO_x/HO_x ratio in determining if smog production would be enhanced or suppressed. However, it was only variations in CH_4 that induced atmospheric changes that could significantly alter atmospheric temperature profiles (through production or lack of production of stratospheric H_2O).

Looking at the 9.6 μm O_3 feature from the simulated emission spectra (Fig. A.4), it is clear that planets around every host star were impacted from the variations in either N_2O either/or CH_4. The cases least affected were around the coolest hosts

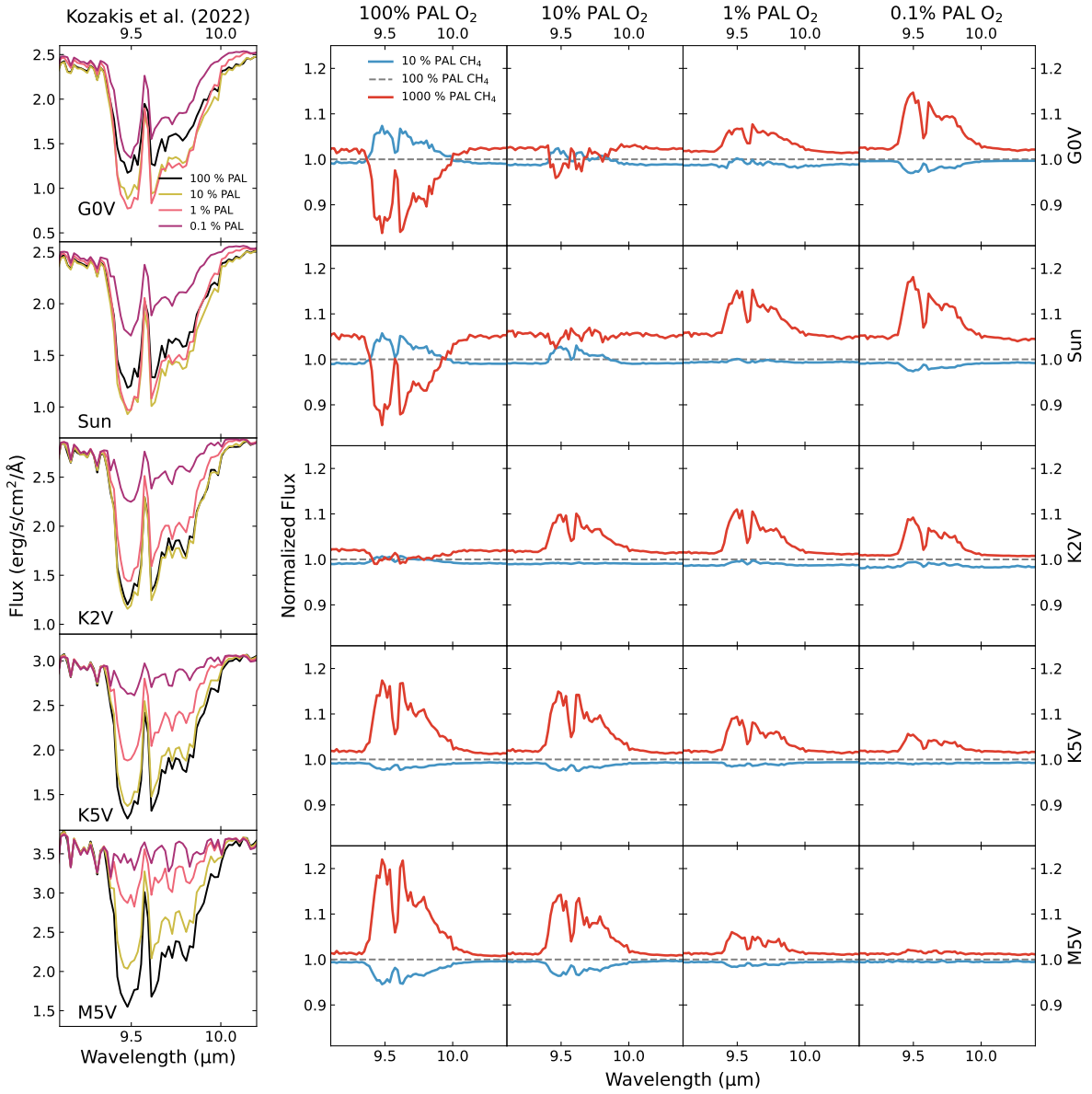

Fig. 8. Comparisons of the 9.6 μm O_3 emission spectra feature for all hosts at different O_2 levels using modern levels of CH_4 (left) and O_3 features for different CH_4 abundances (right) normalized to features with modern levels of CH_4. Normalized O_3 features use the same y-axis limits for all host stars in order to compare the difference in impact of CH_4 on O_3 for different hosts. For the hottest hosts at 100% PAL O_2 changes in feature strength are due to changes in O_3 abundances as well as stratospheric temperatures differences from H_2O abundance, while the rest of the model spectra variations are due mainly to changes in O_3 due to variations in CH_4.

at the lowest O_2 values. The most significant changes overall in the O_3 spectral feature were for the K2V-hosted planet at 100% PAL O_2 with high N_2O, which was ironically the only case that was relatively untouched by CH_4 variations at 100% PAL O_2. Planets around the G0V and Sun hosts faced the most variations in how N_2O and CH_4 impacted the O_3 feature based on the O_2 level, with high N_2O causing shallower features at high O_2 and deeper features at low O_2, with the reverse occurring for the high CH_4 models. We also find that the O_3 feature of the M5V-hosted planet was only significantly changed by variations in CH_4, not in N_2O. Planets around all other hosts experienced spectral feature changes from both N_2O and CH_4 variations to some degree. For future observations it seems that understanding the N_2O and CH_4 content of a planetary atmosphere will be important if we wish to use O_3 as a proxy for O_2, although our results thus far indicate that changes in N_2O will be less relevant for planets around hosts like the M5V star used here, but that CH_4 can have much more of an effect on O_3 abundance.

5.2. Comparisons to other studies

Although this is the first study to vary both O_2 and CH_4 in Earth-like atmospheres orbiting a variety of host stars with the goal of studying the impact on O_3, there are several other studies exploring similar concepts. Grenfell et al. (2006) varies both CH_4 and O_2 abundances (along with NO_x, H_2, and CO) in the context of Proterozoic Earth to evaluate the role of smog-produced O_3 in UV shielding during that time period. They focus on O_2 levels used in this study (10% and 100% PAL O_2) but adopt CH_4 mixing ratios an order of magnitude larger than we used with our high CH_4 models (1.0×10^{-4} and 3.0×10^{-4}). Therefore we

cannot compare directly to our results for the planet around the Sun, but we do see some similar trends. Grenfell et al. (2006) found that NO_x was the main driver in changing O_3 production, but that when NO_x abundances were high enough to enter the NO_x-saturated regime, increasing CH_4 (and therefore HO_x) provided a boost in the smog mechanism. This agrees with our results for the hottest hosts in our study at high O_2 (and therefore the highest NO_x), as we found that increased CH_4 and HO_x helped to counteract NO_x-saturated atmospheres and increased the amount of smog-produced O_3 (see Fig. 6). Despite the different parameter spaces in Grenfell et al. (2006) and this study, both display the same trends of the importance of the NO_x/HO_x ratio determining the efficiency of the smog mechanism, and that in high NO_x environments extra HO_x results in more smog-produced O_3.

Grenfell et al. (2014) also varies CH_4 on an Earth-like planet, but around an M7V host star. They focus on the impact on biosignatures when varying biological surface fluxes of N_2O and CH_4, along with the UV spectrum of the host star, using CH_4 fluxes 100 times less than present day, and 2 and 3 times that of present day. Although they see some similar trends to the work in this study (and results agreeing well with Kozakis et al. 2025) the differences in CH_4 boundary conditions (fixed surface flux rather than fixed mixing ratio) and different UV abundances make it difficult to draw many direct comparisons. That being said, there are no direct contradictions to the findings of this study, with differences in results likely due to different parameter space and boundary conditions.

Searching through the literature we could not find any studies replicating our results of stratospheric cooling via excess H_2O with our high CH_4 models around hotter hosts, although several studies find high amounts of H_2O production in high CH_4 atmospheres (e.g., Segura et al. 2005; Rauer et al. 2011). We do not believe our results of stratospheric cooling contradict any existing studies as this is the first to model such levels of O_2 and CH_4 around hotter hosts, and stratospheric cooling due to greenhouse gases such as CO_2 has been modeled and observed on modern Earth (e.g., Goessling & Bathiany 2016; Santer et al. 2023).

We also note that the decision to use fixed mixing ratios as the boundary condition for certain species (O_2, N_2O, CH_4, H_2, CO) impacts our results differently than if we were to use fixed surface fluxes. As discussed in Kozakis et al. (2022) and Kozakis et al. (2025), species such as N_2O and CH_4 have been shown to build up in the atmospheres of Earth-like planets around cooler host stars due to the low incident UV flux (e.g., Rugheimer et al. 2015; Wunderlich et al. 2019; Teal et al. 2022). In addition, CO abundance (which is strongly interlinked with CH_4 abundance) has been shown to similarly build up in such environments (see Schwieterman et al. 2019 and references therein). We reiterate here that our choice in fixed mixing ratio boundary conditions is to enable easier comparison between the differences in the O_2–O_3 relationship for planets around different host stars. The impact of different boundary conditions will be explored at length in future work.

5.3. Plausible CH_4 mixing ratios in Earth-like atmospheres

The purpose of this study was to further evaluate potential changes in the O_2–O_3 relationship when CH_4 levels are varied, and our choice of using CH_4 abundances of 10% and 1000% PAL was motivated by the need to begin filling out the parameter space over which Earth-like exoplanets may exist. The plausible range of CH_4 in the atmospheres of such planets is still unknown, but we can use our knowledge of CH_4 abundances over the geological history of Earth as a rough guide.

A complication to making such predictions is that surface flux and resulting atmospheric mixing ratios of CH_4 are nonlinear (similar to N_2O), with a strong dependency on the abundance of O_2 and other oxidizing species. O_2 combined with CH_4 is said to be a promising disequilibrium biosignature pair due to the fact that they react quickly with each other and large surface fluxes of O_2 and CH_4 are required to allow significant amounts of both to co-exist in an Earth-like atmosphere. The amount of CH_4 that is able to accumulate in the atmosphere is additionally dependent on the type of host star, where similarly to N_2O, planets around cooler hosts with less incoming UV allow for a larger buildup of CH_4 (e.g., Segura et al. 2003; Rugheimer et al. 2013).

On the early Earth before the Great Oxidation Event CH_4 was likely significantly higher in abundance due to the reducing atmosphere and lack of appreciable O_2, and it is possible that during the Archean era that CH_4 abundances could have been greater than 1000 ppm (e.g., Arney et al. 2016; Catling & Zahnle 2020). Thompson et al. (2022) and Akahori et al. (2024) both modeled surface fluxes of CH_4 to see the corresponding CH_4 atmospheric mixing ratios around the Archean Earth, before the rise of O_2, around the Sun and other spectral hosts. They found that during this time period although there was very little O_2, CH_4 still faced destruction from photolysis and reactions with OH created from H_2O photolysis.

After the rise of O_2 it is possible that there was still a significant amount of CH_4 in the atmosphere, perhaps contributing significantly to the warming of the Proterozoic Earth (Roberson et al. 2011), although it also is possible that there was not significant CH_4 during this era (e.g., Olson et al. 2016). The relationship between CH_4 surface flux and atmospheric mixing ratios has been explored at length in Gregory et al. (2021), which varied both CH_4 and O_2 surface fluxes, as they highly impact the stability of both species in the atmosphere. In Kozakis et al. (2025) we were able to discuss an actual limit of biologically produced N_2O, but with CH_4 there is no known maximum limit of biological CH_4 surface flux. As such, it is unknown how much CH_4 can accumulate in the atmosphere of an O_2-rich planet.

6. Summary and conclusions

This study expands on previous work by considering the impacts of different amounts of atmospheric CH_4 on the O_2–O_3 relationship for an Earth-like planet. We find that the impact of varying CH_4 on the O_2–O_3 relationship is highly influenced by both the host star and the amount of O_2 in the atmosphere, in a manner similar to when N_2O is varied (Kozakis et al. 2025). Increasing CH_4 to 1000% PAL in our high CH_4 models was found to have significantly more of an impact on O_3 than when we decreased CH_4 to 10% PAL with our low CH_4 models (Sect. 4.1). The most striking result is that planets around the hottest hosts with high O_2 abundances (>50% PAL) experienced the opposite response of O_3 to CH_4 to all other models we explored. There are two main reasons for this effect. First, in high UV environments for models with plentiful O_2 and high CH_4 large amounts of stratospheric H_2O were created, which resulted in cooler stratospheres that increased O_3 production and slowed down its destruction, in a process similar to stratospheric cooling via CO_2 on modern Earth. Second, for these hotter hosts at high O_2 there was a boost in O_3-produced smog with the high CH_4 models, as the additional HO_x created from H_2O resulted in a higher NO_x/HO_x

ratio than with modern levels of CH_4. This allowed these "NO_x-saturated" atmospheres to have faster smog mechanisms as it was more difficult for NO_x to lock up the available HO_x into reservoir species. For the hottest hosts at lower O_2 levels, as well as all models around cooler hosts, the high CH_4 models resulted in lower O_3 abundances than compared with modern levels of CH_4. This was primarily due to the increased efficiency of the HO_x catalytic cycle in destroying O_3.

The largest absolute changes in O_3 abundance due to variations in CH_4 occurred at higher O_2 levels, causing the amount of harmful UVC reaching the surface of our model planets to change significantly, especially for the high CH_4 models (Sect. 4.2). At 100% PAL O_2 for the high CH_4 models the planets orbiting the Sun and M5V hosts experienced factors of 7.5×10^{-5} and 2.1×10^4 times the amount of UVC surface flux, respectively, when compared to models with modern levels of CH_4. When considering how this could impact future observations we looked at the 9.6 μm O_3 feature in planetary emission spectra (Sect. 4.3). We found again that the high CH_4 models had the most impact, with planets around all hosts being affected to some degree depending on the amount of O_2 in the atmosphere. Planets orbiting the G0V and Sun hosts with the high CH_4 models had the most change in the O_3 feature dependent on the O_2 level, with the extra CH_4 sometimes causing a deeper or shallower feature.

These results further complicate the usage of O_3 as a proxy for O_2, but also provide additional guidance for future observations. We have now shown in this study that varying CH_4 impacts the O_2–O_3 relationship just as much as N_2O (Kozakis et al. 2025), but in different ways. There are many scenarios where high CH_4 could be increasing the O_3 of an atmosphere, while high N_2O would be working at the same time to deplete that O_3. This shows that we would be required to think about variations of both species in order to use an O_3 measurement to learn about the O_2 content of the atmosphere. Once again we gain no general rules about how O_3 would be impacted when thinking about variations in CH_4 or N_2O, with the specific host star playing a highly influential role.

We find that untangling the impact of CH_4 and N_2O on the O_2–O_3 relationship might be more straightforward for cooler stars, especially around hosts like the M5V star used in this study as N_2O impacts on O_3 are minimal, with CH_4 mainly impacting the atmosphere at higher O_2 abundances. Planets around hotter hosts like our G0V and Sun hosts have the potential to more significantly alter O_3 measurements, as impacts from CH_4 and N_2O on O_3 change significantly based on the O_2 content of the atmosphere. Careful modeling and retrieval studies exploring the parameter space of O_2, N_2O, and CH_4 for Earth-like atmospheres will be necessary if we wish to glean information about the amount of O_3 – and therefore O_2 – in a exoplanetary atmosphere when the time comes that we are able to perform such observations.

Acknowledgements. This project is funded by VILLUM FONDEN and all computing was performed on the HPC cluster at the Technical University of Denmark (DTU Computing Center 2021). Authors TK and LML acknowledge financial support from Severo Ochoa grant CEX2021-001131-S funded by MCIN/AEI/10.13039/501100011033. JMM acknowledges support from the Horizon Europe Guarantee Fund, grant EP/Z00330X/1. We thank the anonymous referee for their useful comments, which improved the clarity of our manuscript.

References

Akahori, A., Watanabe, Y., & Tajika, E. 2024, ApJ, 970, 20
Angerhausen, D., Pidhorodetska, D., Leung, M., et al. 2024, AJ, 167, 128
Arney, G., Domagal-Goldman, S. D., Meadows, V. S., et al. 2016, Astrobiology, 16, 873
Batalha, N. E., Marley, M. S., Lewis, N. K., & Fortney, J. J. 2019, ApJ, 878, 70
Batalha, N., Rooney, C., & MacDonald, R. 2021, https://doi.org/10.5281/zenodo.5093710
Catling, D. C., & Zahnle, K. J. 2020, Sci. Adv., 6, eaax1420
Chapman, S. A. 1930, Mem. R. Met. Soc., 3, 103
Des Marais, D. J., Harwit, M. O., Jucks, K. W., et al. 2002, Astrobiology, 2, 153
Domagal-Goldman, S. D., Segura, A., Claire, M. W., Robinson, T. D., & Meadows, V. S. 2014, ApJ, 792, 90
DTU Computing Center 2021, DTU Computing Center resources, https://doi.org/10.48714/DTU.HPC.0001
Fauchez, T. J., Villanueva, G. L., Schwieterman, E. W., et al. 2020, Nat. Astron., 4, 372
France, K., Loyd, R. O. P., Youngblood, A., et al. 2016, ApJ, 820, 89
Gao, P., Hu, R., Robinson, T. D., Li, C., & Yung, Y. L. 2015, ApJ, 806, 249
Goessling, H. F., & Bathiany, S. 2016, Earth Syst. Dyn., 7, 697
Gregory, B. S., Claire, M. W., & Rugheimer, S. 2021, Earth Planet. Sci. Lett., 561, 116818
Grenfell, J. L., Stracke, B., Patzer, B., Titz, R., & Rauer, H. 2006, Int. J. Astrobiol., 5, 295
Grenfell, J. L., Gebauer, S., v. Paris, P., Godolt, M., & Rauer, H. 2014, Planet. Space Sci., 98, 66
Haagen-Smit, A. J. 1952, Ind. Eng. Chem., 44, 1342
Harman, C. E., Schwieterman, E. W., Schottelkotte, J. C., & Kasting, J. F. 2015, ApJ, 812, 137
Hu, R., Seager, S., & Bains, W. 2012, ApJ, 761, 166
Kasting, J. F. 1979, PhD thesis, University of Michigan, United States
Kasting, J. F., & Ackerman, T. P. 1986, Science, 234, 1383
Kasting, J. F., & Donahue, T. M. 1980, J. Geophys. Res., 85, 3255
Kasting, J. F., Holland, H. D., & Pinto, J. P. 1985, J. Geophys. Res. 90, 10497
Kopparapu, R. K., Ramirez, R., Kasting, J. F., et al. 2013, ApJ, 770, 82
Kozakis, T., Mendonça, J. M., & Buchhave, L. A. 2022, A&A, 665, A156
Kozakis, T., Mendonça, J. M., Buchhave, L. A., & Lara, L. M. 2025, A&A, 699, A247
Kurucz, R. L. 1979, ApJS, 40, 1
Lederberg, J. 1965, Nature, 207, 9
Léger, A., Fontecave, M., Labeyrie, A., et al. 2011, Astrobiology, 11, 335
Lippincott, E. R., Eck, R. V., Dayhoff, M. O., & Sagan, C. 1967, ApJ, 147, 753
Logan, J. A., Prather, M. J., Wofsy, S. C., & McElroy, M. B. 1981, J. Geophys. Res.: Oceans, 86, 7210
Lovelock, J. E. 1965, Nature, 207, 568
Luger, R., & Barnes, R. 2015, Astrobiology, 15, 119
Léger, A., Pirre, M., & Marceau, F. J. 1993, A&A, 277, 309
Meadows, V. S., Arney, G. N., Schwieterman, E. W., et al. 2018a, Astrobiology, 18, 133
Meadows, V. S., Reinhard, C. T., Arney, G. N., et al. 2018b, Astrobiology, 18, 630
Olson, S. L., Reinhard, C. T., & Lyons, T. W. 2016, PNAS, 113, 11447
Quanz, S. P., Absil, O., Benz, W., et al. 2022, Exp. Astron., 54, 1197
Ratner, M. I., & Walker, J. C. G. 1972, J. Atmos. Sci., 29, 803
Rauer, H., Gebauer, S., Paris, P. V., et al. 2011, A&A, 529, A8
Roberson, A. L., Roadt, J., Halevy, I., & F., K. J. 2011, Geobiology, 9, 313
Rugheimer, S., Kaltenegger, L., Zsom, A., Segura, A., & Sasselov, D. 2013, Astrobiology, 13, 251
Rugheimer, S., Kaltenegger, L., Segura, A., Linsky, J., & Mohanty, S. 2015, ApJ, 809, 57
Santer, B. D., Po-Chedley, S., Zhao, L., et al. 2023, PNAS, 120, e2300758120
Schwieterman, E. W., Kiang, N. Y., Parenteau, M. N., et al. 2018, Astrobiology, 18, 663
Schwieterman, E. W., Reinhard, C. T., Olson, S. L., et al. 2019, ApJ, 874, 9
Schwieterman, E. W., Olson, S. L., Pidhorodetska, D., et al. 2022, ApJ, 937, 109
Segura, A., Krelove, K., Kasting, J. F., et al. 2003, Astrobiology, 3, 689
Segura, A., Kasting, J. F., Meadows, V., et al. 2005, Astrobiology, 5, 706
Teal, D. J., Kempton, E. M. R., Bastelberger, S., Youngblood, A., & Arney, G. 2022, ApJ, 927, 90
Thompson, M. A., Krissansen-Totton, J., Wogan, N., Telus, M., & Fortney, J. J. 2022, PNAS, 119, e2117933119
Tian, F., France, K., Linsky, J. L., Mauas, P. J. D., & Vieytes, M. C. 2014, Earth Planet. Sci. Lett., 385, 22
Toon, O. B., McKay, C. P., Ackerman, T. P., & Santhanam, K. 1989, J. Geophys. Res., 94, 16287
Wordsworth, R., & Pierrehumbert, R. 2014, ApJ, 785, L20
Wunderlich, F., Godolt, M., Grenfell, J. L., et al. 2019, A&A, 624, A49
Zahnle, K., Claire, M. W., & Catling, D. 2006, Geobiology, 4, 271

Appendix A: Supplementary figures and tables

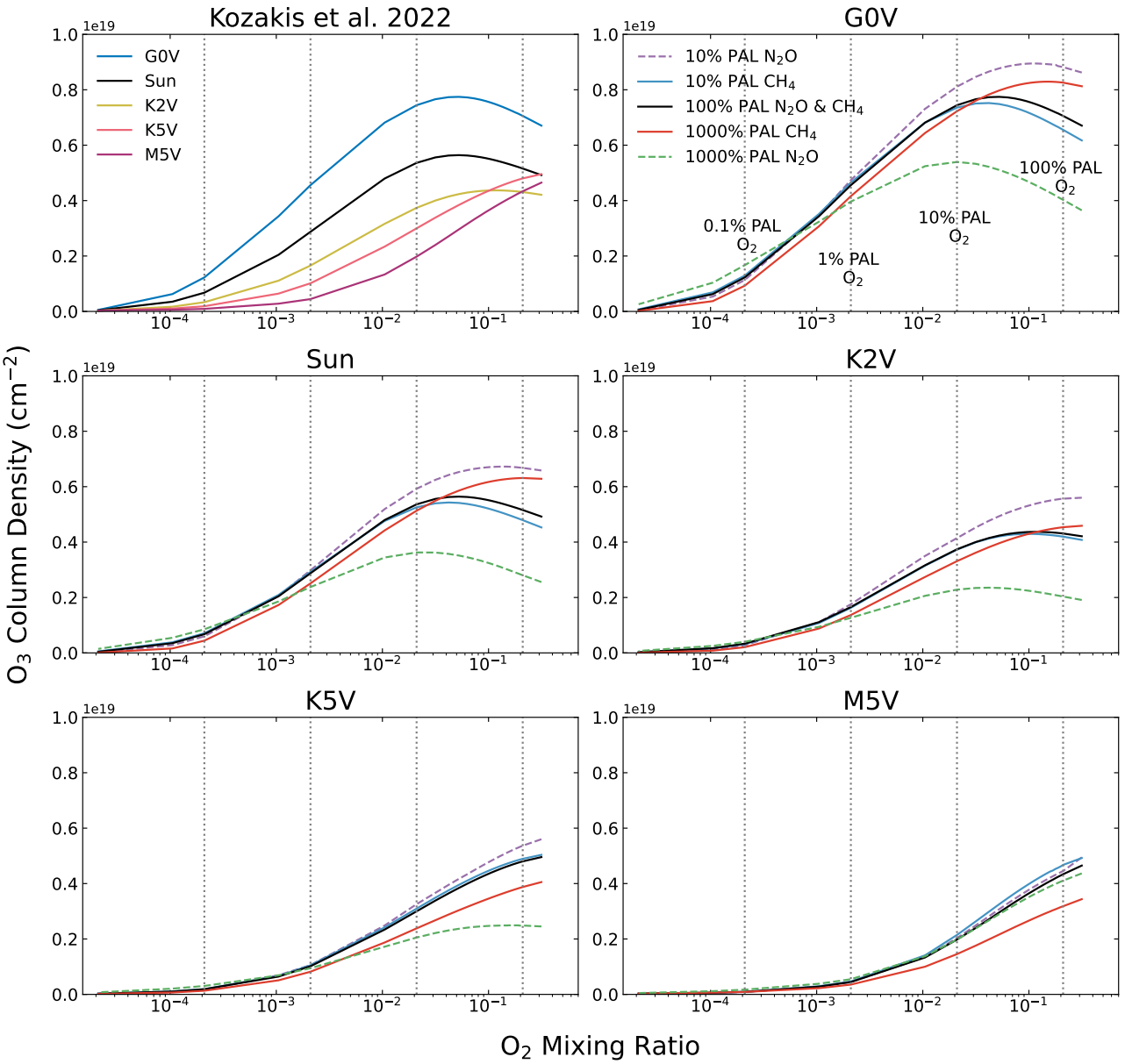

Fig. A.1. Relationships of O_2–O_3 for all host stars at all O_2 and CH_4 levels modeled, along with comparisons to varying levels of N_2O as modeled in Kozakis et al. (2025). All plots share the same y-axis scale to facilitate comparisons. For planets around all hosts except the M5V there are larger variations in O_3 when varying N_2O rather than CH_4. Only the M5V-hosted planet exhibits stronger changes in O_3 with CH_4 variations.

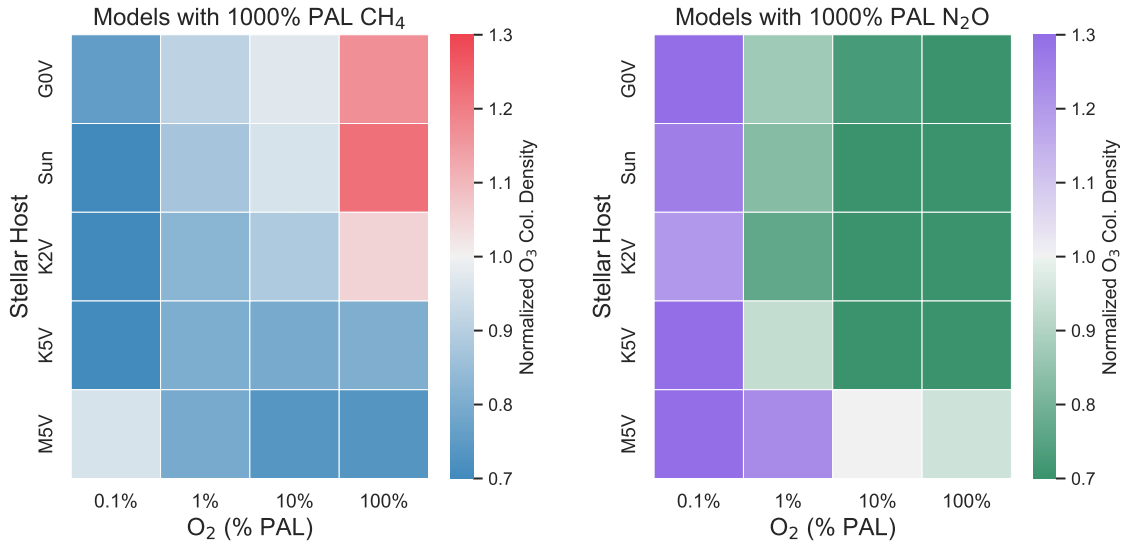

Fig. A.2. Abundances of O_3 for both high CH_4 models from this study and high N_2O models from Kozakis et al. (2025) normalized to the amount of O_3 with modern amounts of CH_4 and N_2O for all host stars at 0.1%, 1%, 10%, and 100% PAL O_2. Both figures share the same color bar limits in order to facilitate comparisons.

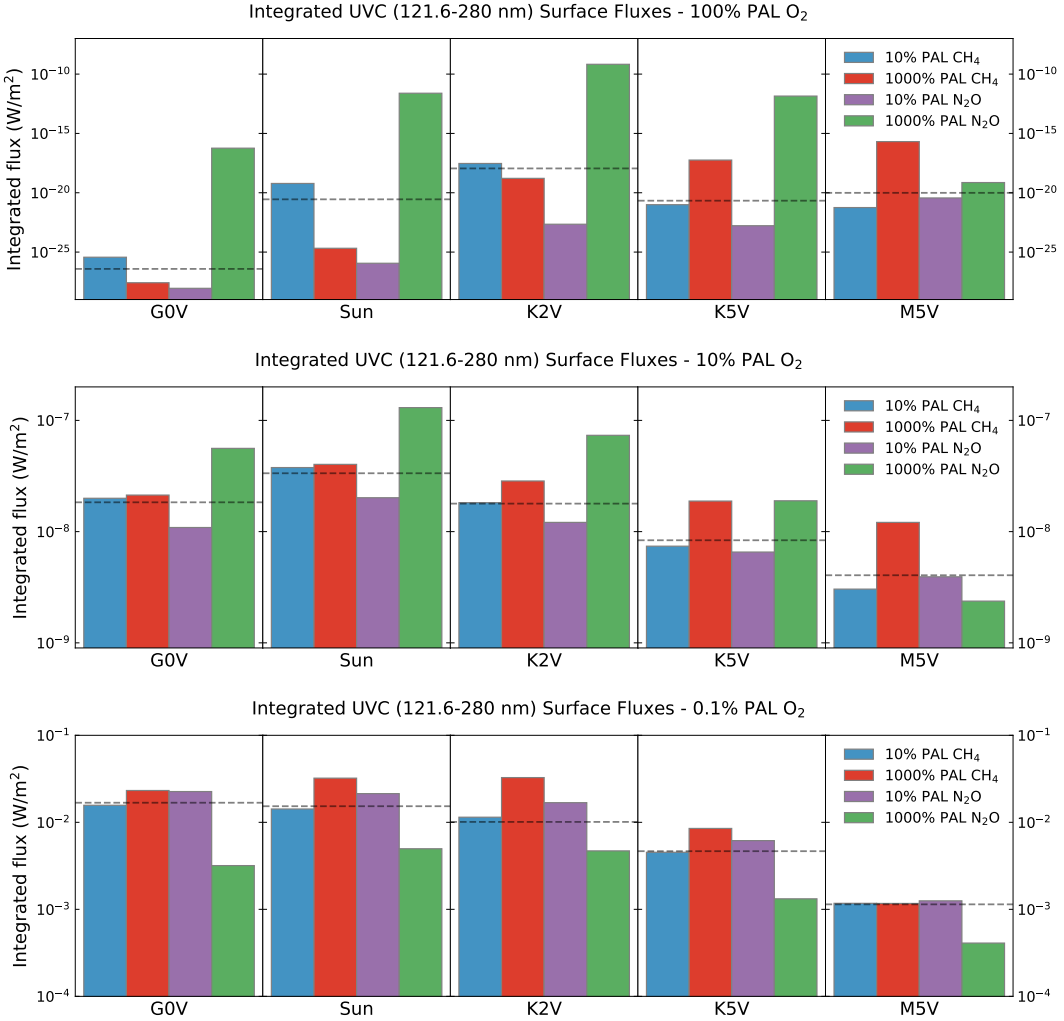

Fig. A.3. Comparisons of UVC surface flux for all hosts at 100%, 10% and 0.1% PAL O_2, as well as high and low CH_4 and N_2O variations from this study as well as Kozakis et al. (2025). The dashed horizontal lines indicate the amount of O_3 for models with modern levels of both CH_4 and N_2O. Overall variations in N_2O have a stronger impact on UVC surface flux, with larger changes when varying CH_4 present primarily at 100% PAL O_2.

Table A.1. UV integrated fluxes

Spectral Type	O_2 MR (% PAL)	TOA flux (W/m^2)	Kozakis et al. (2022) Surface Flux (W/m^2)	Surface Flux Normalized to Kozakis et al. (2022)			
				10% PAL N_2O	1000% PAL N_2O	10% PAL CH_4	1000% PAL CH_4
UVB Fluxes (280–315 nm)							
G0V	100	22.35	1.5e+00	0.72	1.84	1.10	0.81
G0V	10	22.35	1.4e+00	0.88	1.47	1.01	1.05
G0V	1	22.35	2.4e+00	0.97	1.13	0.98	1.09
G0V	0.1	22.35	5.9e+00	1.05	0.84	0.98	1.14
Sun	100	16.18	1.6e+00	0.74	1.69	1.07	0.80
Sun	10	16.18	1.6e+00	0.89	1.43	1.02	1.05
Sun	1	16.18	2.7e+00	0.98	1.13	0.99	1.10
Sun	0.1	16.18	5.6e+00	1.05	0.90	0.98	1.15
K2V	100	4.8	6.8e-01	0.79	1.67	1.02	0.95
K2V	10	4.8	7.4e-01	0.92	1.39	1.00	1.09
K2V	1	4.8	1.2e+00	0.97	1.13	1.01	1.09
K2V	0.1	4.8	2.2e+00	1.04	0.95	1.01	1.10
K5V	100	0.68	9.8e-02	0.90	1.60	0.98	1.19
K5V	10	0.68	1.4e-01	0.95	1.24	0.98	1.15
K5V	1	0.68	2.3e-01	0.99	1.02	0.99	1.07
K5V	0.1	0.68	3.4e-01	1.02	0.92	1.00	1.05
M5V	100	3.5e-02	6.5e-03	0.98	1.04	0.94	1.24
M5V	10	3.5e-02	1.0e-02	0.99	1.00	0.96	1.13
M5V	1	3.5e-02	1.6e-02	1.00	0.96	0.99	1.04
M5V	0.1	3.5e-02	2.0e-02	1.01	0.94	1.00	1.00
UVC Fluxes (121.6–280 nm)							
G0V	100	11.2	3.8e-27	2.3e-02	1.5e+10	9.7e+00	6.8e-02
G0V	10	11.2	1.8e-08	5.9e-01	3.1e+00	1.1e+00	1.2e+00
G0V	1	11.2	1.7e-04	1.0e+00	5.2e-01	9.2e-01	1.4e+00
G0V	0.1	11.2	1.7e-02	1.3e+00	1.9e-01	9.4e-01	1.4e+00
Sun	100	6.7	2.8e-21	4.1e-06	8.8e+08	2.2e+01	7.5e-05
Sun	10	6.7	3.3e-08	6.0e-01	3.9e+00	1.1e+00	1.2e+00
Sun	1	6.7	2.3e-04	1.0e+00	7.2e-01	9.4e-01	1.5e+00
Sun	0.1	6.7	1.5e-02	1.4e+00	3.2e-01	9.3e-01	2.1e+00
K2V	100	1.4	1.1e-18	2.0e-05	6.0e+08	2.6e+00	1.5e-01
K2V	10	1.4	1.8e-08	6.8e-01	4.1e+00	1.0e+00	1.6e+00
K2V	1	1.4	1.0e-04	9.8e-01	8.4e-01	1.0e+00	1.4e+00
K2V	0.1	1.4	1.0e-02	1.7e+00	4.6e-01	1.1e+00	3.2e+00
K5V	100	0.16	2.1e-21	7.8e-03	6.6e+08	4.6e-01	2.7e+03
K5V	10	0.16	8.4e-09	7.8e-01	2.3e+00	8.8e-01	2.3e+00
K5V	1	0.16	5.4e-05	1.0e+00	5.7e-01	9.4e-01	1.5e+00
K5V	0.1	0.16	4.7e-03	1.3e+00	2.8e-01	9.7e-01	1.8e+00
M5V	100	2.7e-02	9.8e-21	3.7e-01	7.4e+00	5.8e-02	2.1e+04
M5V	10	2.7e-02	4.1e-09	9.7e-01	5.9e-01	7.5e-01	3.0e+00
M5V	1	2.7e-02	3.8e-05	1.0e+00	4.0e-01	8.8e-01	1.8e+00
M5V	0.1	2.7e-02	1.1e-03	1.1e+00	3.6e-01	1.0e+00	1.0e+00

Notes. Abbreviations: MR = mixing ratio; PAL = present atmospheric level; TOA = top of atmosphere

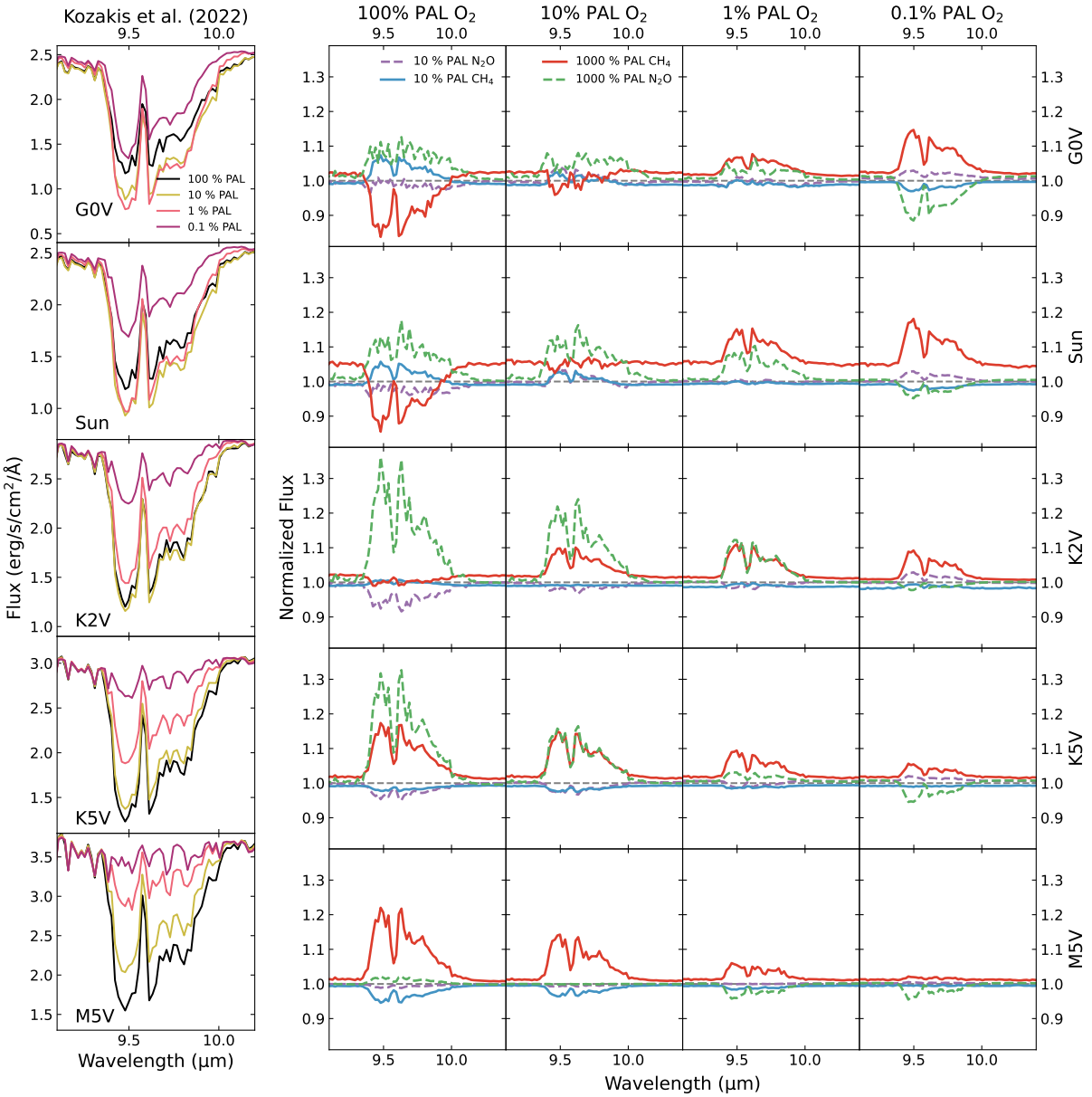

Fig. A.4. Comparisons of 9.6 μm O_3 emission spectra features from Kozakis et al. (2022) with modern levels of CH_4 and N_2O (left) and O_3 features from varying CH_4 and N_2O models normalized to modern amounts of CH_4 and N_2O (right). Y-axis limits for all normalized features are the same to allow for comparison between different O_2 levels and host stars. For both variations in CH_4 and N_2O changes in the O_3 feature were primarily due to differences in O_3 abundance rather than changes in the atmospheric temperature profiles. The exception being for the CH_4 models for the hotter stars at 100% PAL O_2, which experienced stratospheric temperature changes depending on the amount of H_2O produced from CH_4.